Inorganic Chemistry

Article

pubs.acs.org/IC

Mechanistic Insights into the C−H Bond Activation of Hydrocarbons by Chromium(IV) Oxo and Chromium(III) Superoxo Complexes

Kyung-Bin Cho,[†,‡] Hyeona Kang,[†,‡] Jaeyoung Woo,[†] Young Jun Park,[†] Mi Sook Seo,[†] Jaeheung Cho,*[,§] and Wonwoo Nam*[,†]

[†]Department of Chemistry and Nano Science, Center for Biomimetic Systems, Ewha Womans University, Seoul 120-750, Korea

[§]Department of Emerging Materials Science, DGIST, Daegu 711-873, Korea

Supporting Information

ABSTRACT: The mechanism of the C−H bond activation of hydrocarbons by a nonheme chromium(IV) oxo complex bearing an N-methylated tetraazamacrocyclic cyclam (TMC) ligand, $[Cr^{IV}(O)(TMC)(Cl)]^+$ (**2**), has been investigated experimentally and theoretically. In experimental studies, reaction rates of **2** with substrates having weak C−H bonds were found to depend on the concentration and bond dissociation energies of the substrates. A large kinetic isotope effect value of 60 was determined in the oxidation of dihydroanthracene (DHA) and deuterated DHA by **2**. These results led us to propose that the C−H bond activation reaction occurs via a H-atom abstraction mechanism, in which H-atom abstraction of substrates by **2** is the rate-determining step. In addition, formation of a chromium(III) hydroxo complex, $[Cr^{III}(OH)(TMC)(Cl)]^+$ (**3**), was observed as a decomposed product of **2** in the C−H bond activation reaction. The $Cr^{III}OH$ product was characterized unambiguously with various spectroscopic methods and X-ray crystallography. Density functional theory (DFT) calculations support the experimental observations that the C−H bond activation by **2** does not occur via the conventional H-atom-abstraction/oxygen-rebound mechanism and that **3** is the product formed in this C−H bond activation reaction. DFT calculations also propose that **2** may have some $Cr^{III}O^{\bullet-}$ character. The oxidizing power of **2** was then compared with that of a chromium(III) superoxo complex bearing the identical TMC ligand, $[Cr^{III}(O_2)(TMC)(Cl)]^+$ (**1**), in the C−H bond activation reaction. By performing reactions of **1** and **2** with substrates under identical conditions, we were able to demonstrate that the reactivity of **2** is slightly greater than that of **1**. DFT calculations again support this experimental observation, showing that the rate-limiting barrier for the reaction with **2** is slightly lower than that of **1**.

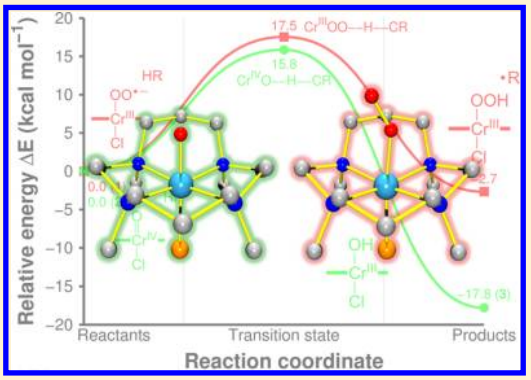

INTRODUCTION

The C−H bond activation of hydrocarbons by metal-bound active oxygen species, such as superoxo, peroxo, hydroperoxo, and oxo, is one of the most important subjects in bioinorganic and oxidation chemistry.[1,2] Among the metal-active oxygen species, high-valent metal oxo intermediates have attracted particular attention as reactive species in the C−H bond activation reactions by enzymes and synthetic catalysts. For instance, high-valent iron(IV) oxo intermediates in heme and nonheme iron enzymes and their models have been intensively investigated to elucidate mechanism(s) of the C−H bond activation by the iron oxo oxidants.[2−4] In heme enzymes such as cytochrome P450 and iron porphyrin models, the C−H bond activation by iron(IV) oxo porphyrin π-cation radicals, $(Porp^{\bullet+})Fe^{IV}{=}O$ (Cpd I), occurs via a rate-determining H-atom abstraction step (Scheme 1A, pathway a), followed by an oxygen-rebound step between the resulting $(Porp)Fe^{IV}OH$ and substrate radical species (Scheme 1A, pathway b).[5] This oxygen-rebound mechanism has been supported strongly in both experiments and theoretical calculations.[6,7] In nonheme iron and manganese models, it has been shown very recently that there is an alternative to the oxygen-rebound mechanism in the C−H bond activation by nonheme iron(IV) oxo and manganese(IV) oxo complexes.[8] That is, the dissociation of the substrate radical (Scheme 1B, pathway c), which is formed by H-atom abstraction by the nonheme iron(IV) oxo and manganese(IV) oxo complexes (Scheme 1B, pathway a), is more favorable than the oxygen-rebound process (Scheme 1B, pathway b). Thus, the latter result casts doubt that the C−H bond activation by high-valent metal oxo species occurs invariably via the conventional H-atom-abstraction/oxygen-rebound mechanism (Scheme 1).

Much attention has recently been focused on the reactivities of metal superoxo species because the intermediates are postulated to be involved as reactive species in the C−H bond activation reactions by copper enzymes (e.g., peptidylglycine-α-amidating monooxygenase and dopamine β-monooxygenase)[9] and nonheme iron enzymes (e.g., isopenicillin N synthase, *myo*-inositol oxygenase, and 2-hydroxyethyl phospho-

Received: November 12, 2013

   dx.doi.org/10.1021/ic402831f | *Inorg. Chem.* XXXX, XXX, XXX−XXX

Scheme 1. Proposed Mechanisms of C−H Bond Activation

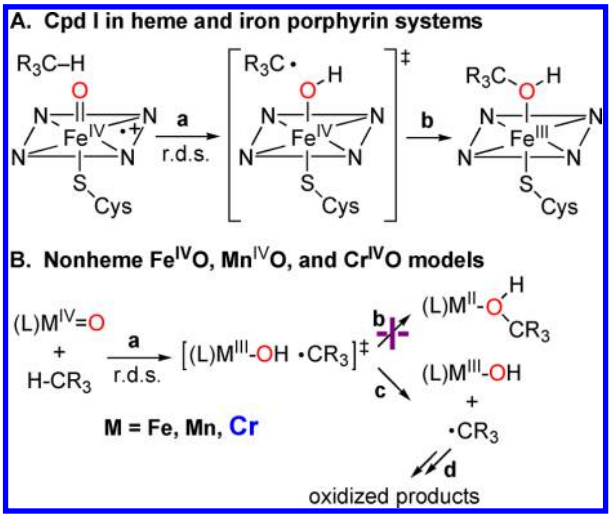

nate dioxygenase).[10] In biomimetic studies, it has been shown that synthetic copper(II) superoxo complexes are capable of performing C−H bond functionalization of a supporting ligand and weak O−H and N−H bond activation of external substrates.[11] In nonheme iron models, although iron(III) superoxo intermediates have been proposed as active oxidants in the course of O_2 activation, no direct evidence for the iron(III) superoxo species participating in the C−H bond activation of hydrocarbons has been obtained yet, probably because of the nature of its instability and short lifetime.[12] The lack of direct evidence for the heme and nonheme iron(III) superoxo species in experiments was complemented by density functional theory (DFT) calculations, in which the nonheme iron(III) superoxo species is shown to be an electrophilic oxidant in H-atom-abstraction reactions, whereas the heme iron(III) superoxo species is a sluggish oxidant in oxidation reactions.[13−15] In addition, a comparison of the oxidizing power of heme and nonheme iron(IV) oxo and iron(III) superoxo intermediates in the C−H bond activation reactions has been another topic that could be addressed in the computational studies.[13]

Very recently, a chromium(III) superoxo complex bearing an N-methylated tetraazamacrocyclic ligand, $[Cr^{III}(O_2)(TMC)(Cl)]^+$ (**1**, where TMC = 1,4,8,11-tetramethyl-1,4,8,11-tetraazacyclotetradecane; Chart 1), was successfully synthesized

Chart 1

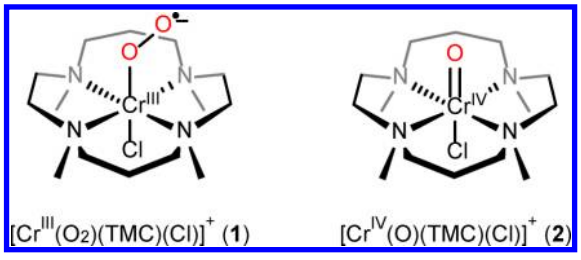

by reacting a chromium(II) precursor with O_2.[16a] The intermediate **1** was thermally stable so that we were able to isolate and use it directly in spectroscopic and structural characterization as well as in reactivity studies. For example, it has been shown that **1** is capable of conducting electrophilic oxidative reactions, such as the activation of weak C−H bonds of hydrocarbons and the O-atom transfer (OAT) to substrates (e.g., the oxidation of phosphine and sulfides).[16] In the latter reaction, a high-valent chromium(IV) oxo complex, $[Cr^{IV}(O)(TMC)(Cl)]^+$ (**2**; Chart 1), was successfully isolated as a product and characterized with various spectroscopic methods and X-ray crystallography.[16b]

As part of our ongoing efforts to understand the mechanism of the C−H bond activation by nonheme metal oxo complexes, we now report for the first time a combined experimental and computational study on the mechanism of the C−H bond activation of hydrocarbons by a nonheme chromium(IV) oxo complex and the direct reactivity comparison of the chromium(III) superoxo and chromium(IV) oxo complexes bearing a common supporting ligand in C−H bond activation reactions carried out under identical conditions.

RESULTS AND DISCUSSION

Experimental Studies on the C−H Bond Activation by Chromium(IV) Oxo and Chromium(III) Superoxo Complexes. The chromium(IV) oxo complex **2** was prepared by reacting its corresponding chromium(III) superoxo complex, **1**, with 1 equiv of PPh_3.[16b] The intermediate **2** was stable enough to be used in reactivity studies under stoichiometric conditions (e.g., $t_{1/2}$ of ∼40 min at −10 °C).[17] Upon the addition of cyclohexadiene (CHD) to the solution of **2** in CH_3CN at −10 °C, the characteristic UV−vis absorption bands of **2** disappeared with a pseudo-first-order decay profile (Figure 1a), and product analysis of the reaction solution revealed that benzene (43 ± 2% based on **2**) was produced as a sole product in the oxidation of CHD (see the Experimental Section). Clean isosbestic points were observed at 527, 574, 615, and 755 nm in this reaction (Figure 1a). A pseudo-first-order fitting of the

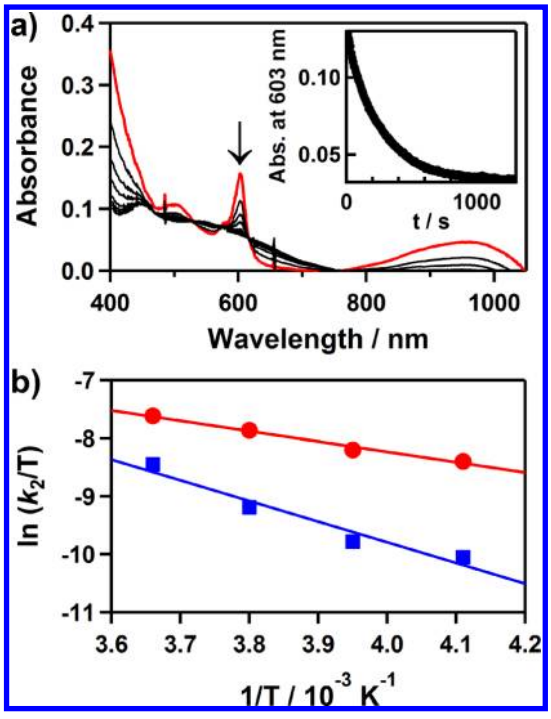

Figure 1. (a) UV−vis spectral changes of **2** (2 mM) upon the addition of CHD (20 equiv to **2**, 40 mM) in CH_3CN at −10 °C. Inset: time course of the decay of **2** monitored at 603 nm. (b) Plot of k_2 against $1/T$ to determine the activation parameters for the reactions of CHD with **1** (blue ■) and **2** (red ●).

dx.doi.org/10.1021/ic402831f | Inorg. Chem. XXXX, XXX, XXX−XXX

kinetic data gave a k_{obs} value of 3.8×10^{-3} s^{-1}. The rate constant increased linearly with an increase of the CHD concentration, affording a second-order rate constant (k_2) of 9.6×10^{-2} M^{-1} s^{-1} at −10 °C (Figure 2a). The reaction rate

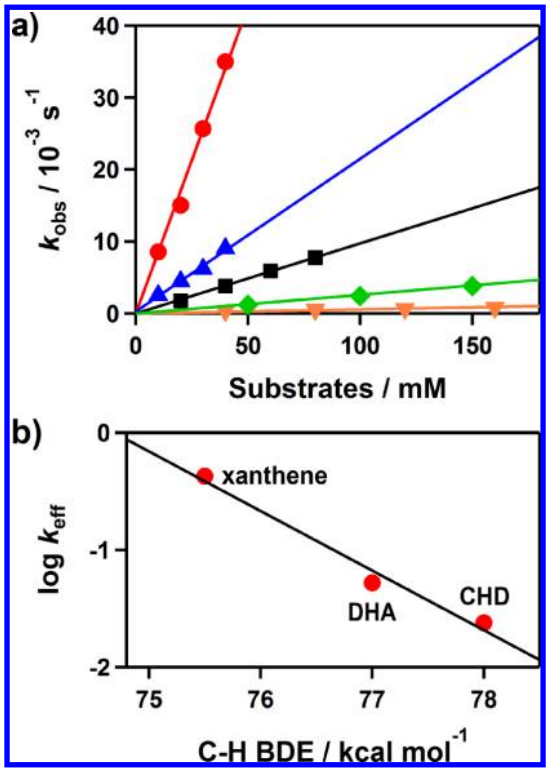

Figure 2. Reaction of **2** with external substrates in CH_3CN at −10 °C. (a) Plots of k_{obs} of **2** against the concentration of xanthene (red ●, $k_2 = 8.6 \times 10^{-1}$ M^{-1} s^{-1}), DHA (blue ▲, $k_2 = 2.1 \times 10^{-1}$ M^{-1} s^{-1}), DHA-d_4 (orange ▼, $k_2 = 3.5 \times 10^{-3}$ M^{-1} s^{-1}), and CHD (black ■, $k_2 = 9.6 \times 10^{-2}$ M^{-1} s^{-1}) to determine second-order rate constants. A plot of k_{obs} of **1** against the concentration of CHD (green ◆, $k_2 = 2.7 \times 10^{-2}$ M^{-1} s^{-1}) under the same reaction condition has also been added. (b) Plot of log k_{eff} of **2** against C−H BDEs of xanthene, DHA, and CHD, showing a correlation of the reaction rates with the BDEs of the substrates. The k_2 values are adjusted for reaction stoichiometry to yield k_{eff} based on the number of equivalent target C−H bonds of the substrates.

was dependent on the reaction temperature, and a linear Eyring plot was obtained in the range of 243−273 K with activation parameters of $\Delta H^{\ddagger} = 3.5$ kcal mol^{-1} and $\Delta S^{\ddagger} = -49.5$ cal mol^{-1} K^{-1} (Figure 1b, red line).

In order to gain mechanistic insight into the C−H bond activation by **2**, we carried out the reaction of **2** with other substrates having weak C−H bond dissociation energies (BDEs), such as xanthene (75.5 kcal mol^{-1}) and 9,10-dihydroanthracene (DHA; 77 kcal mol^{-1}) along with CHD (78 kcal mol^{-1}),[18] from which second-order rate constants were determined [Figure 2a; Supporting Information (SI), Table S1]. Product analysis of the reaction solutions revealed that xanthone (45 ± 5% based on **2**) and anthracene (42 ± 2% based on **2**) were produced in the oxidation of xanthene and DHA, respectively. The rate constants decreased with an increase of the C−H BDEs of the substrates, giving a linear correlation with the C−H BDE values of the substrates (Figure 2b). We also observed a large deuterium kinetic isotope effect (KIE) value of 60(6) in the oxidation of DHA and DHA-d_4 by **2** (see the data with blue and orange colors in Figure 2a). Such a large KIE value suggests a tunneling behavior in the H-atom-abstraction reaction, as is frequently observed in H-atom-abstraction reactions by iron(IV) oxo intermediates of nonheme iron enzymes and models.[19] It is worth noting that **1** also gave a high KIE value (~50) in the C−H bond activation of DHA.[16a] On the basis of the observations of the linear correlation between the reaction rates and BDEs of the substrates and the large KIE value, we propose that the C−H bond activation by **2** occurs via a H-atom-abstraction mechanism and that the H-atom abstraction is the rate-determining step, as observed in other metal oxo reactions.[8,19,20]

By analysis of the reaction solution of **2** and CHD with cold spray ionization time-of-flight mass spectrometry (CSI-TOF MS), we found that a chromium(III) hydroxo complex, **3**, was formed as a decomposed product of **2** in the C−H bond activation reaction (Figure 3a). We also found an O atom in the

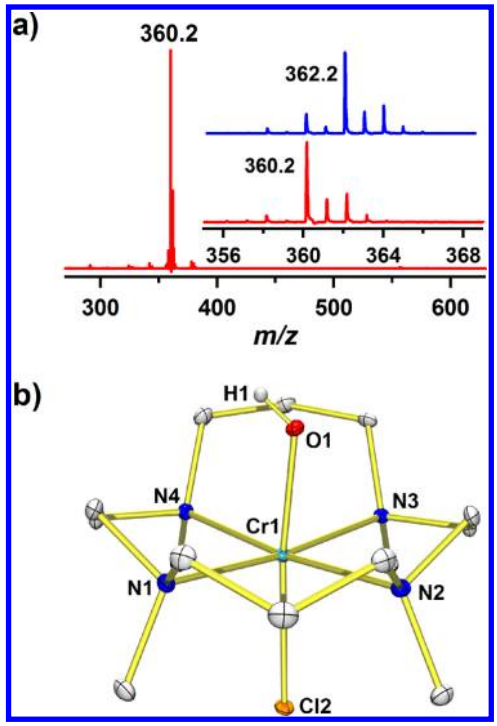

Figure 3. (a) CSI-TOF MS showing the formation of **3** in the reaction of **2** and CHD in CH_3CN at −10 °C. Insets: observed isotope distribution patterns for $[Cr^{III}(^{16}OH)(TMC)(Cl)]^+$ at m/z 360.2 and $[Cr^{III}(^{18}OH)(TMC)(Cl)]^+$ at m/z 362.2. (b) ORTEP plot of **3** with a 30% probability thermal ellipsoid. All H atoms except H1 are omitted for clarity. The hydroxyl proton was found in the Fourier difference map. Selected bond lengths (Å) and angles (deg): Cr−O1 1.8630(12), Cr−N1 2.1316(13), Cr−N2 2.1607 (13), Cr−N3 2.1746(14), Cr−N4 2.1477(13), Cr−Cl2 2.3731(4); O1−Cr−Cl2 173.50(4).

OH group of the $Cr^{III}OH$ product derived from the oxo group in **2** by carrying out an ^{18}O isotope labeling experiment with $[Cr^{IV}(^{18}O)(TMC)(Cl)]^+$ (**2**-^{18}O; Figure 3a, upper inset). The X-ray crystal structure of **3**-Cl·CH_3CN·H_2O revealed that the hydroxide ligand coordinates to the chromium center, affording a distorted octahedral geometry with a Cr−O bond distance of 1.8630(12) Å (Figure 3b; SI, Tables S2 and S3). On the basis of the structural and spectroscopic characterization of **3**, we were able to conclude unambiguously that a $Cr^{III}OH$ complex is the product formed in the C−H bond activation of

dx.doi.org/10.1021/ic402831f | Inorg. Chem. XXXX, XXX, XXX−XXX

hydrocarbons by a nonheme chromium(IV) oxo complex.[21] We have shown previously that $Fe^{III}OH$ and $Mn^{III}OH$ are the products formed in the C−H bond activation of hydrocarbons by nonheme iron(IV) oxo and manganese(IV) oxo complexes, respectively.[8] On the basis of the present results, we propose that the C−H bond activation by the $Cr^{IV}O$ complex does not occur via an oxygen-rebound mechanism (Scheme 1B, pathway b). Instead, dissociation of the substrate radical is more favorable than the oxygen-rebound process (Scheme 1B, pathway c), giving the $Cr^{III}OH$ complex product.[22] A similar mechanism was proposed in the C−H bond activation of hydrocarbons by nonheme iron(IV) oxo and manganese(IV) oxo complexes.[8]

We then compared the reactivities of the chromium(III) superoxo (**1**) and chromium(IV) oxo (**2**) complexes in the C−H bond activation of hydrocarbons under identical reaction conditions (e.g., in CH_3CN and at −10 °C). In these reactions, **2** showed a slightly greater reactivity, compared to that of **1** (SI, Table S1).[23] For example, in the CHD oxidation, **2** (k_2 = 9.6 × 10^{-2} M^{-1} s^{-1}) was 3.6 times more reactive than **1** (k_2 = 2.7 × 10^{-2} M^{-1} s^{-1}; Figure 2a, black and green lines; also compare the data in the SI, Table S1). A linear Eyring plot, obtained in the range of 243−273 K for the reaction of **1** and CHD, afforded activation parameters of $\Delta H^{‡}$ = 7.1 kcal mol^{-1} and $\Delta S^{‡}$ = −38.2 cal mol^{-1} K^{-1} (Figure 1b). The $\Delta\Delta G$ value of 0.6 kcal mol^{-1}, which was calculated from the activation parameters of **1** and **2**, supports the greater reactivity of **2** in the C−H bond activation reaction (see the SI, Table S4; vide infra). As observed in the reaction of **2**, **3** was the product formed in the C−H bond activation of hydrocarbons by **1**.[16a] We propose that the formation of **3** occurs via the formation of an intermediate **2** in the C−H bond activation by **1**. Because the reactivity of **2** is greater than that of **1**, **2** is not detected in this reaction. Finally, it is worth noting that a chromium(V) oxo complex bearing the same TMC ligand showed a much lower reactivity than both **1** and **2** in the C−H bond activation reactions, although the axial ligand of the chromium(V) oxo complex was different from that of **1** and **2** [e.g., methoxide for chromium(V) oxo vs chloride for **1** and **2**].[24]

Theoretical Calculations on the C−H Bond Activation by Chromium(IV) Oxo and Chromium(III) Superoxo Complexes. The reactivities of **1** and **2** in the C−H activation reaction were investigated with DFT as well. CHD was used as a substrate in both cases. The calculated transition-state (TS) structures of **1** and **2** in the initial C−H bond activation reactions are shown in Figure 4. Spin contamination issues have been reviewed for both **1** and **2**, which are presented in the SI.

The optimized geometry of **1** without the substrate shows a root-mean-square deviation (RMSD) of 0.28 Å compared to the crystal structure, indicating a fair agreement with experiments. The ground state of **1** was calculated to be S = 1, which is also in agreement with experiments.[25] The orbitals involved in this structure are reminiscent of what has been described earlier for iron(III) superoxo species.[13c] Figure 5 shows a schematic diagram of the valence orbitals involved and their occupations, where the z axis denotes the Cr−O bond direction and the x axis denotes the projected direction of the O−O bond that is perpendicular to the z axis. The simplest way to analyze the orbitals is to consider the structure as a binding between S = 2 of Cr^{II} and S = 1 of O_2. The five valence orbitals (here denoted as d_{xy}, d_{xz}, d_{yz}, $\sigma^*_{z^2}$, and σ^*_{xy} in **1**) are usually the ones considered active. In Cr^{II}, d_{xy}, d_{xz}, d_{yz}, and $\sigma^*_{z^2}$ are singly occupied, whereas σ^*_{xy} is unoccupied. From the O_2 side, the

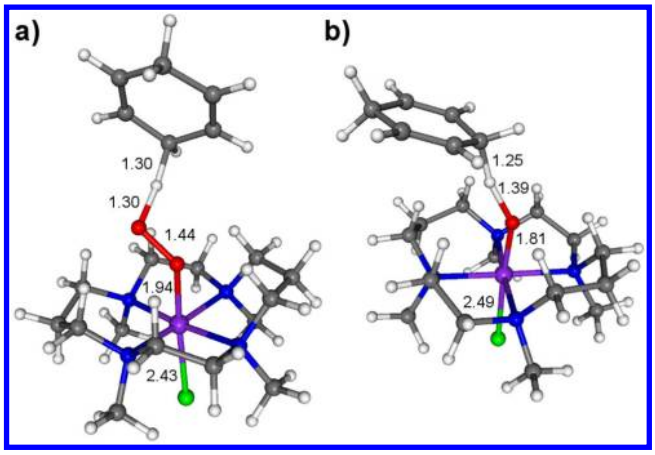

Figure 4. TS structures of (a) **1** and (b) **2** performing C−H abstraction reactions in the S = 1 spin state. Selected bond lengths are given in angstroms.

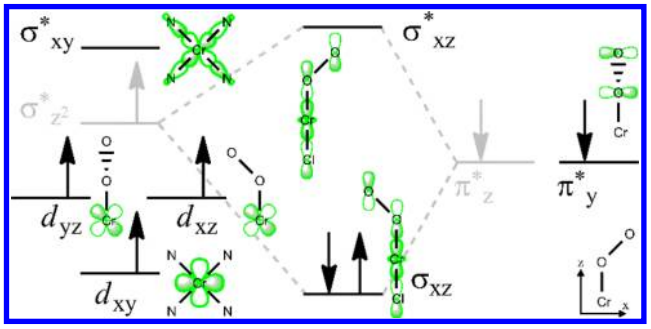

Figure 5. Five valence orbitals d_{xy}, d_{xz}, d_{yz}, $\sigma^*_{z^2}$, and σ^*_{xy} from the (Cl)Cr^{II}(TMC) moiety (left) and the two O_2 orbitals π^*_y and π^*_z (right). In the $[Cr^{III}(OOH)(TMC)(Cl)]^+$ complex, the $\sigma^*_{z^2}$ and π^*_z orbitals (in gray) mix to form two new σ-type bonding (σ_{xz}) and antibonding (σ^*_{xz}) orbitals, where the former one becomes doubly occupied. The d_{yz} and π^*_y orbitals also mix in a similar fashion, but this mixing is weak and is therefore best described as an antiferromagnetic coupling rather than an orbital mixing and pairing.

π^*_z and π^*_y orbitals of the triplet oxygen are each singly occupied by β electrons. Upon complexation, the orbitals from both sides mix with each other (d_{yz} with π^*_y and d_{z^2} with π^*_z). We find that d_{yz} with π^*_y mixing is weak in the S = 1 state of **1**. A complete pairing of the α electron in d_{yz} with the β electron in π^*_y is not seen because the superoxo moiety has a spin-density distribution of −0.97 (SI, Table S9). Therefore, this "pairing" is more correctly described as an antiferromagnetic pairing rather than orbital mixing. However, this antiferromagnetic coupling is not negligible, as is shown by the energy of its ferromagnetic counterpart (S = 2), which is 5.3 kcal mol^{-1} higher in energy. In contrast, the d_{z^2} and π^*_z mixing creates two new orbitals (σ_{xz} and σ^*_{xz} in Figure 5), where electron pairing occurs in the bonding σ_{xz} orbital. This bonding orbital has 49% contribution from the O_2 moiety and 32% from the Cr d orbital, with the rest coming from the TMC and Cl ligands. Therefore, **1** is from a strict electron spatial distribution point of view more correctly described as a $Cr^{II}O_2$ moiety, which happens to have an unpaired electron count that matches that of the chromium(III) superoxo species. Mulliken spin-density distribution indeed shows about 3.3 in α spin on Cr (SI, Table S9), seemingly implicating a high-spin Cr^{III} antiferromagnetically coupled to a superoxo species. Hence, the exact oxidation state of the metal depends on the point of view. We follow in

dx.doi.org/10.1021/ic402831f | Inorg. Chem. XXXX, XXX, XXX−XXX

this paper the latter convention because of its relevance to spectroscopical assignments.

The C−H bond activation by **1** was investigated in three spin states (S = 0, 1, and 2). The S = 0 state was found to have high energies throughout the reaction and was ruled out (see the SI, Table S7). The calculated electronic energy barrier for the reaction for S = 1 was 17.5 kcal mol^{-1}. The S = 2 state, while not ruled out, has a higher TS at 18.7 kcal mol^{-1}. Electronic energy barriers in this range are expected to be close to the experimental free-energy values,[26] and indeed the experimentally measured activation barrier is 17.2 kcal mol^{-1} at −10 °C (SI, Table S4). This reaction is slightly exergonic (−2.7 kcal mol^{-1}), forming a [Cr^{III}(OOH)(TMC)(Cl)]$^+$ species that can react further to form intermediate **2**. At this intermediate stage, the electron abstracted from the substrate resides in the π^*_y orbital. The orbital occupation of the Cr side remains the same, implicating an $S = {}^3/_2$ chromium(III) hydroperoxo character. Including the substrate spin, the S = 1 structure differs from the S = 2 state only by the spin direction on the now-formed substrate radical. This is also seen by the degenerate energies of these states (−2.6 kcal mol^{-1} for both).

For **2**, the calculated ground-state spin is also S = 1 (see the SI, Table S6), in agreement with experiments.[16b] Comparing the calculated structure to the crystal one, the obtained RMSD is 0.26 Å. Interestingly, Mulliken spin-density distribution shows spins on Cr and O of 2.71 and −0.46, respectively (SI, Table S10). We can explain this spin polarization by orbital mixing here as well. The starting point is to consider the CrO complex as a mix of Cr^{III} and O$^{\bullet-}$. Figure 6 (red) shows that, in this configuration, there are three unpaired α electrons on the Cr side (d_{xz}, d_{yz}, and d_{xy}) and one unpaired β electron on the oxo side (p_x). The expected spin-density distributions in this case on Cr and O are 3 and −1, respectively. Upon orbital mixing, d_{xz} mixes with p_x to form the bonding and antibonding orbital pair denoted as π_{xz} and π^*_{xz}, respectively. Similarly, π_{yz}, π^*_{yz}, σ_{z^2}, and $\sigma^*_{z^2}$ are formed by mixing the other orbitals (Figure 6, gray arrows). If the mixing is complete, each of these orbitals will have 50% contribution from both Cr and O (Figure 6, blue). In this case, the unpaired electron count gives that the expected spin-density distribution would be 1.5 on Cr and 0.5 on O. Our calculated spin-density values fall between these extreme points (pure Cr^{III}O$^{\bullet-}$ and pure Cr^{IV}O). Hence, the calculations seem to suggest that the supposedly Cr^{IV}O species, in fact, has some Cr^{III}O$^{\bullet-}$ character mixed into it. Extensive investigation into whether these are calculation artifacts (so-called spin contamination) has been detailed in the SI. The result of this investigation is that this inclusion of some Cr^{III}O$^{\bullet-}$ character is more consistent with the crystal structure than pure Cr^{IV}O. Also, this is reminiscent of calculations on any Fe^{IV}O species (supposedly 3/0 in spin density on Fe/O), which is widely known to give spin-density distribution more consistent with Fe^{III}O$^{\bullet-}$ (i.e., 2/1).[26] However, the exact nature of this compound is immaterial to our conclusions below even though it remains to be conclusively experimentally determined. The orbital discussion below is therefore based on the simplified Cr^{IV}O view, where the orbital mixings are complete.

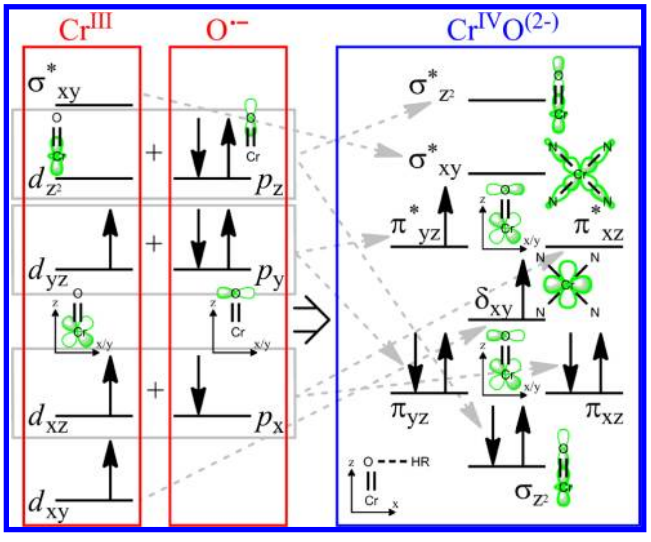

Figure 6. Valence orbitals of **2** such as Cr^{III}O$^{\bullet-}$ (red) or Cr^{IV}O (blue) for the S = 1 state. The d_{z^2} orbital of Cr can mix with the p_z orbital of O to form the bonding and antibonding pair of orbitals σ_{z^2} and $\sigma^*_{z^2}$ (gray). Similarly, d_{xz} mixes with p_x to form π_{xz}/π^*_{xz} and d_{yz} mixes with p_y to form π_{yz}/π^*_{yz}. Depending on how well these orbitals from Cr and O mix with each other, the CrO compound can be characterized as anything between pure Cr^{III}O$^{\bullet-}$ (no mixing) to Cr^{IV}O (evenly mixed).

Upon C−H bond activation by **2**, one α electron is transferred from the substrate to the empty π^*_{xz} orbital together with the proton. The Cr^{III}OH moiety is most stable at the $S = {}^3/_2$ state, coupled to a β spin on the substrate (in total S = 1). Also, like in the case of **1**, the reactivity on the S = 0 state (leading to $S = {}^1/_2$ Cr^{III}OH coupled to a β-spin substrate) is ruled out because of the high energies (see the SI, Table S8). The initial C−H bond activation on the S = 1 state occurs over a barrier of 15.8 kcal mol^{-1}, close to the experimental value of 16.6 kcal mol^{-1}. Thus, **2** is calculated to have a lower barrier than **1** (Figure 7), and the calculations are in agreement with experiments showing a greater reactivity for **2** (vide supra). The reaction ends in a stable intermediate **3** (RMSD = 0.18 Å to the crystal structure, with the only significant difference being the O−H direction).

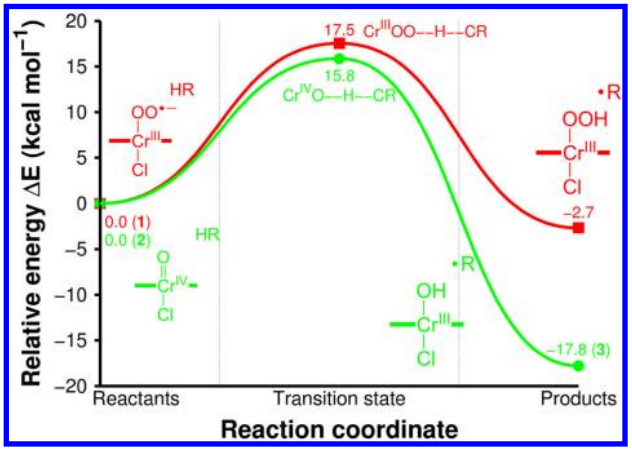

Figure 7. Comparison of the rate-limiting barriers in the C−H activation reactions of CHD by **1** (red) versus **2** (green).

For the ensuing steps after this initial C−H bond activation by **2**, one can envision four scenarios in the cage (i.e., [(L)M^{III}OH$^{\bullet}$CR$_3$]‡ in Scheme 1B):[8] (1) a rebound step where **3** returns its OH to the CHD radical to form a hydroxylated product (Scheme 1B, pathway b), (2) further abstraction of a H atom from the substrate radical by **3** to form water and benzene (i.e., desaturation), (3) simply a dissociation of the substrate radical to react with a second catalyst **2** (Scheme 1B, pathways

dx.doi.org/10.1021/ic402831f | Inorg. Chem. XXXX, XXX, XXX−XXX

c and d), or (4) a substrate spin flip to obtain an overall $S = 2$ spin state that has a lower desaturation barrier. As noted earlier in the similar $Mn^{III}OH$ case,[8c] a spin flip for an organic radical is likely a relatively slow process[27] compared to other options available, especially dissociation (vide infra). Hence, we do not consider the fourth option feasible for this reaction as whole. The three remaining pathways are depicted in Figure 8. We

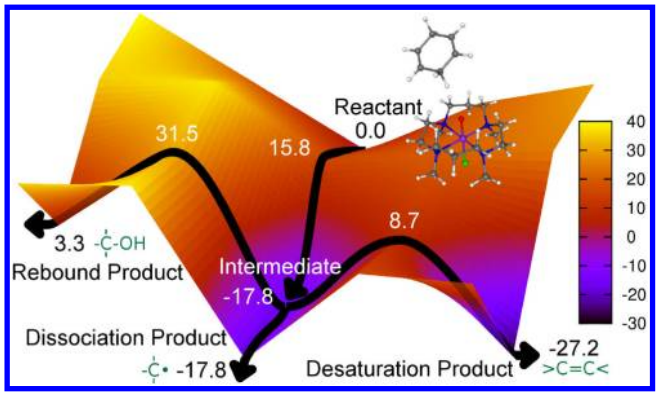

Figure 8. Potential energy surface on the $S = 1$ surface of **2** performing a C−H abstraction reaction (far end) to form the hydroxylated intermediate **3** (center). The energy barriers for the rebound (left) and desaturation (right) reactions are high, whereas the dissociation reaction (near end) is thermoneutral.

have shown earlier that, in C−H bond activation reactions by both nonheme $Fe^{IV}O$ and $Mn^{IV}O$ species, the third option is preferable,[8b,c] which can be experimentally verified by detecting Mn^{III}/Fe^{III} products instead of Mn^{II}/Fe^{II} products, with a substrate product yield of 50% relative to the catalyst. Our calculated barrier values for the rebound (49.3 kcal mol^{-1} relative to the intermediate), desaturation (26.4 kcal mol^{-1}), and dissociation (0.03 kcal mol^{-1}) reactions confirm that the substrate radical dissociation from the cage is a preferred pathway in the case of $Cr^{IV}O$ as well. The relatively high barriers for the rebound and desaturation reactions reflect the lack of driving force in these reactions. The desaturation reaction is only 9.4 kcal mol^{-1} exergonic (in the $S = 1$ spin state), and the rebound process is even endergonic by 21.1 kcal mol^{-1}. While these values (and TSs; see the SI, Table S8) are considerably lower in the $S = 2$ state because of favorable exchange interactions between the unpaired spins,[28] as mentioned earlier, spin flip to the $S = 2$ state should still not be able to compete with dissociation. These results are all in agreement with the results discussed in the Experimental Section, such as the observation of $Cr^{III}OH$ as the metal product together with 45% organic product (vide supra).

CONCLUSIONS

Mechanistic studies of the C−H bond activation of hydrocarbons by nonheme chromium(III) superoxo and chromium(IV) oxo complexes bearing a common supporting ligand, **1** and **2**,[16] were performed under stoichiometric conditions. In the C−H bond activation by the chromium(IV) oxo complex, we have shown that the C−H bond activation reaction occurs via a H-atom-abstraction mechanism. We have also demonstrated that the C−H bond activation does not occur via the conventional H-atom-abstraction/oxygen-rebound mechanism.[5−7] Instead, dissociation of the substrate radical formed via H-atom abstraction from the substrate is more favorable than the oxygen-rebound process, as we have shown in both nonheme iron(IV) oxo and manganese(IV) oxo reactions.[8] These results are supported by DFT calculations, showing that the energy barrier of the substrate radical dissociation is much lower than those of the oxygen-rebound and desaturation processes.

We have also shown that the reactivity patterns of the nonheme chromium(III) superoxo and chromium(IV) oxo complexes are similar in the C−H bond activation reactions. For example, the H-atom abstractions by the chromium(III) superoxo and chromium(IV) oxo complexes are the rate-determining steps, and large KIE values were obtained in these reactions. By comparing their reactivities under identical reaction conditions, the reactivity of the chromium(IV) oxo complex was found to be slightly greater than that of the chromium(III) superoxo complex in the C−H bond activation reactions. Theoretical calculations have shown that the energy difference between the TSs for the C−H bond activation reactions of CHD by the chromium(III) superoxo and chromium(IV) oxo complexes is 1.7 kcal mol^{-1}, which is in reasonable agreement with the experimental result (0.6 kcal mol^{-1}). In addition, the calculations show that the chromium(IV) oxo species may have some $Cr^{III}O^{\bullet-}$ character mixed, although future verifications are needed through experiments and accurate ab initio calculations. Finally, the present results provide clues that may help us understand the role(s) of the metal oxo and metal superoxo intermediates involved in C−H bond activation reactions by nonheme iron and copper enzymes.[9,10]

EXPERIMENTAL SECTION

Materials. All chemicals obtained from Aldrich Chemical Co. were the best available purity and used without further purification unless otherwise indicated. Solvents were dried according to published procedures and distilled under argon prior to use.[29] $^{18}O_2$ (98% ^{18}O-enriched) was purchased from ICON Services Inc. (Summit, NJ). The deuterated substrate, DHA-d_4, was prepared by taking DHA (0.5 g, 2.7 mmol) in DMSO-d_6 (3 mL) along with NaH (0.2 g, 8.1 mmol) under an inert atmosphere.[30] After the deep-red solution was stirred at room temperature for 8 h, the reaction was quenched with D_2O (5 mL). The crude product was filtered and washed with copious amounts of H_2O. ^1H NMR confirmed the >99% deuteration of DHA-d_4. **1**-Cl·$(CH_3CN)_2$ and **2**-Cl·CH_3CN·H_2O were prepared according to literature methods.[16]

Physical Methods. UV−vis spectra were recorded on a Hewlett-Packard 8453 diode-array spectrophotometer equipped with a UNISOKU Scientific Instrument for low-temperature experiments. Cold spray ionization time-of-flight mass spectrometry (CSI-TOF MS) spectra were collected on a JMS-T100CS (JEOL) mass spectrometer equipped with a CSI source. Typical measurement conditions are as follows: needle voltage, 2.2 kV; orifice 1 current, 50−500 nA; orifice 1 voltage, 0−20 V; ring lens voltage. 10 V; ion source temperature, 5 °C; spray temperature, −30 °C. The CSI-TOF MS of **3** was observed by directly infusing the reaction solution into the ion source through a precooled tube under high air gas pressure. Product analysis was performed with an Agilent Technologies 6890N gas chromatograph and a Thermo Finnigan (Austin, TX) FOCUS DSQ (dual-stage quadrupole) mass spectrometer interfaced with a Finnigan FOCUS gas chromatograph (GC−MS). ^1H NMR spectra were measured with a Bruker DPX-400 spectrometer. The effective magnetic moments were determined using the modified ^1H NMR method of Evans at −10 °C.[31] A WILMAD coaxial insert (sealed capillary) tubes containing the blank acetonitrile-d_3 solvent (with 1.0% tetramethylsilane, TMS) only was inserted into the normal NMR tubes containing the complexes (8 mM) dissolved in acetonitrile-d_3 (with 0.05% TMS). The chemical shift of the TMS peak (and/or

dx.doi.org/10.1021/ic402831f | Inorg. Chem. XXXX, XXX, XXX−XXX

solvent peak) in the presence of the paramagnetic metal complexes was compared to that of the TMS peak (and/or solvent peak) in the inner coaxial insert tube. The effective magnetic moment was calculated using the equation $\mu = 0.0618(\Delta\nu T/2fM)^{1/2}$, where f is the oscillator frequency (MHz) of the superconducting spectrometer, T is the absolute temperature, M is the molar concentration of the metal ion, and $\Delta\nu$ is the difference in frequency (Hz) between the two reference signals.[31]

X-ray Crystallography. Single crystals of **3**-Cl·CH_3CN·H_2O were picked from solutions by a nylon loop (Hampton Research Co.) on a handmade copper plate mounted inside a liquid N_2 Dewar vessel at ca. −40 °C and mounted on a goniometer head in a N_2 cryostream. Data collections were carried out on a Bruker SMART APEX II CCD diffractometer equipped with a monochromator in the Mo Kα (λ = 0.71073 Å) incident beam. The CCD data were integrated and scaled using the Bruker *SAINT* software package, and the structure was solved and refined using *SHELXTL V 6.12*.[32] H atoms were located in the calculated positions except H1 in a hydroxyl group, which was found from the Fourier difference map. All non-H atoms were refined with anisotropic thermal parameters. Crystal data for **3**-Cl·CH_3CN·H_2O: $C_{16}H_{38}Cl_2CrN_5O_2$: monoclinic, $P2_1$, Z = 2, a = 7.35270(10) Å, b = 9.7682(2) Å, c = 14.9867(2) Å, β = 94.8750(10)°, V = 1072.49(3) Å^3, μ = 0.803 mm^{-1}, ρ_{calcd} = 1.410 g cm^{-3}, R1 = 0.0235, wR2 = 0.0497 for 5146 unique reflections, 252 variables. CCDC-942471 for **3**-Cl·CH_3CN·H_2O contain the supplementary crystallographic data for this paper. These data can be obtained free of charge via www.ccdc.cam.ac.uk/data_request/cif (or from the Cambridge Crystallographic Data Centre, 12 Union Road, Cambridge CB2 1EZ, U.K.; fax (+44) 1223-336-033 or e-mail deposit@ccdc.cam.ac.uk).

Generation and Characterization of 3-Cl·CH_3CN·H_2O. The treatment of **2**, which was obtained by the reaction of [Cr^{II}(TMC)-(Cl)](Cl)·$(CH_3CN)_2$ (23.1 mg, 0.05 mmol), excess O_2, and 1 equiv of PPh_3 in CH_3CN (1 mL) at −10 °C,[16b] with 10 equiv of CHD afforded formation of a light-yellow solution. Single crystals suitable for X-ray analysis were obtained from layering of diethyl ether on top of the reaction solution at −40 °C. Yield: 19.5 mg (80%). UV−vis [λ, nm (ε, M^{-1} cm^{-1})] in CH_3CN at −10 °C (Figure 1a): 360 (330), 440 (160), 540 (110). CSI-MS in CH_3CN at −10 °C (Figure 3a): m/z 360.2110 for **3** (calcd m/z 360.1748).

Reactivity Studies. All reactions were run by monitoring UV−vis spectral changes of reaction solutions, and rate constants were determined by fitting changes in absorbance at 603 nm for **2**. Reactions were run at least in triplicate, and the data reported represent the average of these reactions. Typically, complex **2**, prepared by treating **1** with 1 equiv of PPh_3 in CH_3CN at −10 °C, was directly used in kinetic studies by adding appropriate amounts of substrates. After the reactions were completed, pseudo-first-order fitting of the kinetic data allowed us to determine the k_{obs} values. The purity of the substrates was checked with GC and GC−MS prior to use. Products were analyzed by injecting the reaction mixture directly into GC and GC−MS. Products were identified by comparison with authentic samples, and product yields were determined by comparison against standard curves prepared with authentic samples and using decane as an internal standard.

DFT Calculations. Calculations were performed at the B3LYP/6-311+G(d,p)//LANL2DZ(6-311G* on Cl) level,[33] with solvent (acetonitrile) modeled through the CPCM scheme[34] (also included during the optimizations), using and as implemented in the *Gaussian 09* package.[35] The energies reported are electronic energies only because free-energy calculations in solvent-included optimized systems introduce a formal error[26,36] (nevertheless, calculated ΔG values are reported in the SI). Spin contamination issues were investigated using a restricted open-shell approach where applicable as well as spin-projected DFT.[37] Even though there are arguments about using the latter procedure,[38] it remains one of the few DFT tools available to use when spin contamination is suspected and the restricted open-shell approach is not applicable. We have also used single-point B2PLYP[39]//UBLYP to evaluate the spin contamination because double hybrids may yield more accurate results with regard to this issue.[40]

■ ASSOCIATED CONTENT

Supporting Information

X-ray crystallographic data in CIF format, experimental and DFT details, Figure S1, Table S1−S16, DFT-calculated coordinates, and the full reference for ref 35 (as ref S3). This material is available free of charge via the Internet at http://pubs.acs.org.

■ AUTHOR INFORMATION

Corresponding Authors

*E-mail: jaeheung@dgist.ac.kr.
*E-mail: wwnam@ewha.ac.kr.

Author Contributions

‡These authors contributed equally.

Notes

The authors declare no competing financial interest.

■ ACKNOWLEDGMENTS

The research was supported by NRF/MEST of Korea through the CRI (Grant 2-2012-1794-001-1) and GRL (Grant 2010-00353) programs (to W.N.), Basic Research Program (Grant 2010-0002558 to M.S.S.), and the R&D programs (Grants 13-BD-0403 and 2013K2A2A4000610 to J.C.).

■ REFERENCES

(1) (a) Solomon, E. I.; Brunold, T. C.; Davis, M. I.; Kemsley, J. N.; Lee, S.-K.; Lehnert, N.; Neese, F.; Skulan, A. J.; Yang, Y.-S.; Zhou, J. *Chem. Rev.* **2000**, *100*, 235−349. (b) Meunier, B., Ed. *Metal−Oxo and Metal−Peroxo Species in Catalytic Oxidations*; Springer: Berlin, 2000. (c) Abu-Omar, M. M.; Loaiza, A.; Hontzeas, N. *Chem. Rev.* **2005**, *105*, 2227−2252. (d) Nam, W. *Acc. Chem. Res.* **2007**, *40*, 465. and review articles in the special issue. (e) Gunay, A.; Theopold, K. H. *Chem. Rev.* **2010**, *110*, 1060−1081. (f) Warren, J. J.; Tronic, T. A.; Mayer, J. M. *Chem. Rev.* **2010**, *110*, 6961−7001. (g) Cho, J.; Sarangi, R.; Nam, W. *Acc. Chem. Res.* **2012**, *45*, 1321−1330. (h) Huynh, M. H. V.; Meyer, T. J. *Chem. Rev.* **2007**, *107*, 5004−5064. (i) Mayer, J. M. *Acc. Chem. Res.* **2011**, *44*, 36−46.

(2) (a) Denisov, I. G.; Makris, T. M.; Sligar, S. G.; Schlichting, I. *Chem. Rev.* **2005**, *105*, 2253−2277. (b) van Eldik, R. *Coord. Chem. Rev.* **2007**, *251*, 1649−1662. (c) Shaik, S.; Hirao, H.; Kumar, D. *Acc. Chem. Res.* **2007**, *40*, 532−542. (d) Bruijnincx, P. C. A.; van Koten, G.; Klein Gebbink, R. J. M. *Chem. Soc. Rev.* **2008**, *37*, 2716−2744. (e) Krebs, C.; Fujimori, D. G.; Walsh, C. T.; Bollinger, J. M., Jr. *Acc. Chem. Res.* **2007**, *40*, 484−492. (f) Nam, W. *Acc. Chem. Res.* **2007**, *40*, 522−531.

(3) (a) Ortiz de Montellano, P. R. *Cytochrome P450: Structure, Mechanism, and Biochemistry*, 3rd ed.; Kluwer Academic/Plenum Publishers: New York, 2005. (b) Shaik, S.; Hirao, H.; Kumar, D. *Acc. Chem. Res.* **2007**, *40*, 532−542. (c) Green, M. T. *Curr. Opin. Chem. Biol.* **2009**, *13*, 84−88. (d) Rittle, J.; Green, M. T. *Science* **2010**, *330*, 933−937.

(4) (a) Borovik, A. S. *Chem. Soc. Rev.* **2011**, *40*, 1870−1874. (b) de Visser, S. P.; Rohde, J.-U.; Lee, Y.-M.; Cho, J.; Nam, W. *Coord. Chem. Rev.* **2013**, *257*, 381−393.

(5) (a) Groves, J. T. *J. Chem. Educ.* **1985**, *62*, 928−931. (b) Groves, J. T. *Proc. Natl. Acad. Sci. U. S. A.* **2003**, *100*, 3569−3574. (c) Groves, J. T. *J. Inorg. Biochem.* **2006**, *100*, 434−447.

(6) (a) Groves, J. T.; McClusky, G. A. *J. Am. Chem. Soc.* **1976**, *98*, 859−861. (b) Groves, J. T.; Van Der Puy, M. *J. Am. Chem. Soc.* **1976**, *98*, 5290−5297. (c) Hjelmeland, L. M.; Aronow, L.; Trudell, J. *Biochem. Biophys. Res. Commun.* **1977**, *76*, 541−549. (d) Gelb, M. H.; Heimbrook, D. C.; Malkonen, P.; Sligar, S. G. *Biochemistry* **1982**, *21*, 370−377.

(7) (a) Ogliaro, F.; Harris, N.; Cohen, S.; Filatov, M.; de Visser, S. P.; Shaik, S. *J. Am. Chem. Soc.* **2000**, *122*, 8977−8989. (b) Guallar, V.; Baik, M.-H.; Lippard, S. J.; Friesner, R. A. *Proc. Natl. Acad. Sci. U. S. A.* **2003**, *100*, 6998−7002. (c) Kamachi, T.; Yoshizawa, K. *J. Am. Chem.*

Soc. **2003**, *125*, 4652−4661. (d) Schöneboom, J. C.; Cohen, S.; Lin, H.; Shaik, S.; Thiel, W. *J. Am. Chem. Soc.* **2004**, *126*, 4017−4034. (e) de Visser, S. P. *J. Am. Chem. Soc.* **2006**, *128*, 9813−9824. (f) Comba, P.; Maurer, M.; Vadivelu, P. *J. Phys. Chem. A* **2008**, *112*, 13028−13036. (g) Hirao, H.; Que, L., Jr.; Nam, W.; Shaik, S. *Chem.—Eur. J.* **2008**, *14*, 1740−1756. (h) Geng, C.; Ye, S.; Neese, F. *Angew. Chem., Int. Ed.* **2010**, *49*, 5717−5720.

(8) (a) Wu, X.; Seo, M. S.; Davis, K. M.; Lee, Y.-M.; Chen, J.; Cho, K.-B.; Pushkar, Y. N.; Nam, W. *J. Am. Chem. Soc.* **2011**, *133*, 20088−20091. (b) Cho, K.-B.; Wu, X.; Lee, Y.-M.; Kwon, Y. H.; Shaik, S.; Nam, W. *J. Am. Chem. Soc.* **2012**, *134*, 20222−20225. (c) Cho, K.-B.; Shaik, S.; Nam, W. *J. Phys. Chem. Lett.* **2012**, *3*, 2851−2856. (d) Hong, S.; So, H.; Yoon, H.; Cho, K.-B.; Lee, Y.-M.; Fukuzumi, S.; Nam, W. *Dalton Trans.* **2013**, *42*, 7842−7845.

(9) (a) Prigge, S. T.; Eipper, B. A.; Mains, R. E.; Amzel, L. M. *Science* **2004**, *304*, 864−867. (b) Chen, P.; Solomon, E. I. *Proc. Natl. Acad. Sci. U. S. A.* **2004**, *101*, 13105−13110. (c) Klinman, J. P. *J. Biol. Chem.* **2006**, *281*, 3013−3016. (d) Rolff, M.; Tuczek, F. *Angew. Chem., Int. Ed.* **2008**, *47*, 2344−2347.

(10) (a) Bollinger, J. M., Jr.; Krebs, C. *Curr. Opin. Chem. Biol.* **2007**, *11*, 151−158. (b) van der Donk, W. A.; Krebs, C.; Bollinger, J. M., Jr. *Curr. Opin. Struct. Biol.* **2010**, *20*, 673−683.

(11) (a) Kunishita, A.; Ertem, M. Z.; Okubo, Y.; Tano, T.; Sugimoto, H.; Ohkubo, K.; Fujieda, N.; Fukuzumi, S.; Cramer, C. J.; Itoh, S. *Inorg. Chem.* **2012**, *51*, 9465−9480. (b) Peterson, R. L.; Himes, R. A.; Kotani, H.; Suenobu, T.; Tian, L.; Siegler, M. A.; Solomon, E. I.; Fukuzumi, S.; Karlin, K. D. *J. Am. Chem. Soc.* **2011**, *133*, 1702−1705. (c) Kunishita, A.; Kubo, M.; Sugimoto, H.; Ogura, T.; Sato, K.; Takui, T.; Itoh, S. *J. Am. Chem. Soc.* **2009**, *131*, 2788−2789. (d) Maiti, D.; Lee, D.-H.; Gaoutchenova, K.; Würtele, C.; Holthausen, M. C.; Narducci Sarjeant, A. A.; Sundermeyer, J.; Schindler, S.; Karlin, K. D. *Angew. Chem., Int. Ed.* **2008**, *120*, 88−91. (e) Maiti, D.; Fry, H. C.; Woertink, J. S.; Vance, M. A.; Solomon, E. I.; Karlin, K. D. *J. Am. Chem. Soc.* **2007**, *129*, 264−265. (f) Cramer, C. J.; Tolman, W. B. *Acc. Chem. Res.* **2007**, *40*, 601−608. (g) Würtele, C.; Gaoutchenova, E.; Harms, K.; Holthausen, M. C.; Sundermeyer, J.; Schindler, S. *Angew. Chem., Int. Ed.* **2006**, *45*, 3867−3869. (h) Itoh, S. *Curr. Opin. Chem. Biol.* **2006**, *10*, 115−122.

(12) (a) Lee, Y.-M.; Hong, S.; Morimoto, Y.; Shin, W.; Fukuzumi, S.; Nam, W. *J. Am. Chem. Soc.* **2010**, *132*, 10668−10670. (b) Mukherjee, A.; Cranswick, M. A.; Chakrabarti, M.; Paine, T. K.; Fujisawa, K.; Münck, E.; Que, L., Jr. *Inorg. Chem.* **2010**, *49*, 3618−3628.

(13) (a) Chung, L. W.; Li, X.; Hirao, H.; Morokuma, K. *J. Am. Chem. Soc.* **2011**, *133*, 20076−20079. (b) Cho, K.-B.; Chen, H.; Janardanan, D.; de Visser, S. P.; Shaik, S.; Nam, W. *Chem. Commun.* **2012**, *48*, 2189−2191. (c) Chen, H.; Cho, K.-B.; Lai, W.; Nam, W.; Shaik, S. *J. Chem. Theory Comput.* **2012**, *8*, 915−926.

(14) (a) Chung, L. W.; Li, X.; Sugimoto, H.; Shiro, Y.; Morokuma, K. *J. Am. Chem. Soc.* **2008**, *130*, 12299−12309. (b) Hirao, H.; Morokuma, K. *J. Am. Chem. Soc.* **2009**, *131*, 17206−17214. (c) Chung, L. W.; Li, X.; Sugimoto, H.; Shiro, Y.; Morokuma, K. *J. Am. Chem. Soc.* **2010**, *132*, 11993−12005. (d) Hirao, H.; Morokuma, K. *J. Am. Chem. Soc.* **2010**, *132*, 17901−17909.

(15) Lai, W.; Shaik, S. *J. Am. Chem. Soc.* **2011**, *133*, 5444−5452.

(16) (a) Cho, J.; Woo, J.; Nam, W. *J. Am. Chem. Soc.* **2010**, *132*, 5958−5959. (b) Cho, J.; Woo, J.; Nam, W. *J. Am. Chem. Soc.* **2012**, *134*, 11112−11115.

(17) We found that **3** is a decomposed product of **2**, which is confirmed by electrospray ionization mass spectrometry (data not shown).

(18) (a) Luo, Y.-R. *Handbook of bond dissociation energies in organic compounds*; CRC Press: New York, 2003. (b) Roth, J. P.; Mayer, J. M. *Inorg. Chem.* **1999**, *38*, 2760−2761. (c) Lam, W. W. Y.; Man, W.-L.; Lau, T.-C. *Coord. Chem. Rev.* **2007**, *251*, 2238−2252.

(19) (a) Price, J. C.; Barr, E. W.; Glass, T. E.; Krebs, C.; Bollinger, J. M., Jr. *J. Am. Chem. Soc.* **2003**, *125*, 13008−13009. (b) Kaizer, J.; Klinker, E. J.; Oh, N. Y.; Rohde, J.-U.; Song, W. J.; Stubna, A.; Kim, J.; Münck, E.; Nam, W.; Que, L., Jr. *J. Am. Chem. Soc.* **2004**, *126*, 472−473. (c) Oh, N. Y.; Suh, Y.; Park, M. J.; Seo, M. S.; Kim, J.; Nam, W. *Angew. Chem., Int. Ed.* **2005**, *44*, 4235−4239. (d) Sastri, C. V.; Lee, J.; Oh, K.; Lee, Y. J.; Lee, J.; Jackson, T. A.; Ray, K.; Hirao, H.; Shin, W.; Halfen, J. A.; Kim, J.; Que, L., Jr.; Shaik, S.; Nam, W. *Proc. Natl. Acad. Sci. U. S. A.* **2007**, *104*, 19181−19186. (e) England, J.; Martinho, M.; Farquhar, E. R.; Frisch, J. R.; Bominaar, E. L.; Münck, E.; Que, L., Jr. *Angew. Chem., Int. Ed.* **2009**, *48*, 3622−3626. (f) England, J.; Guo, Y.; Farquhar, E. R.; Young, V. G., Jr.; Münck, E.; Que, L., Jr. *J. Am. Chem. Soc.* **2010**, *132*, 8635−8644. (g) Xue, G.; Hont, R. D.; Münck, E.; Que, L., Jr. *Nat. Chem.* **2010**, *2*, 400−405. (h) Seo, M. S.; Kim, N. H.; Cho, K.-B.; So, J. E.; Park, S. K.; Clémancey, M.; Garcia-Serres, R.; Latour, J.-M.; Shaik, S.; Nam, W. *Chem. Sci.* **2011**, *2*, 1039−1045.

(20) (a) Mayer, J. M. *Acc. Chem. Res.* **1998**, *31*, 441−450. (b) Borovik, A. S. *Acc. Chem. Res.* **2005**, *38*, 54−61. (c) Gardner, K. A.; Kuehnert, L. L.; Mayer, J. M. *Inorg. Chem.* **1997**, *36*, 2069−2078. (d) Matsuo, T.; Mayer, J. M. *Inorg. Chem.* **2005**, *44*, 2150−2158. (e) Lam, W. W. Y.; Yiu, S. M.; Yiu, D. T. Y.; Lau, T. C.; Yip, W. P.; Che, C. M. *Inorg. Chem.* **2003**, *42*, 8011−8018. (f) Goldsmith, C. R.; Cole, A. P.; Stack, T. D. P. *J. Am. Chem. Soc.* **2005**, *127*, 9904−9912.

(21) Qin, K.; Incarvito, D. I.; Rheingold, A. L.; Theopold, K. H. *J. Am. Chem. Soc.* **2002**, *124*, 14008−14009.

(22) We rule out the possibility that the formation of the $Cr^{III}OH$ product does not result from comproportionation of Cr^{IV}=O and Cr^{II} (see the SI, Figure S1), as we have shown in the reactions of nonheme iron(IV) oxo and manganese(IV) oxo complexes. See refs 8a and 8b.

(23) It is of interest to note that **2** is inactive in OAT reactions (i.e., the oxidation of PPh_3 and sulfides). This is how **2** was prepared by reacting **1** with either PPh_3 or thioanisole. See ref 16b.

(24) Cho, J.; Woo, J.; Han, J. E.; Kubo, M.; Ogura, T.; Nam, W. *Chem. Sci.* **2011**, *2*, 2057−2062.

(25) The S = 1 ground state of **1** was confirmed by using the ^{1}H NMR spectroscopic method of Evans; the magnetic moment is 3.0(2) μ_B. See the Experimental Section for details.

(26) Cho, K.-B.; Kim, E. J.; Seo, M. S.; Shaik, S.; Nam, W. *Chem.—Eur. J.* **2012**, *18*, 10444−10453.

(27) Gould, I. R.; Turro, N. J.; Zimmt, M. B. In *Advances in Physical Organic Chemistry*; Gold, V., Bethell, D., Eds.; Academic Press: New York, 1984; Vol. *20*, pp 1−53.

(28) Shaik, S.; Chen, H.; Janardanan, D. *Nat. Chem.* **2011**, *3*, 19−27; *Nat. Chem.* **2011**, *4*, 511.

(29) Armarego, W. L. F., Perrin, D. D., Eds. *Purification of Laboratory Chemicals*; Pergamon Press: Oxford, U.K., 1997.

(30) Goldsmith, C. R.; Jonas, R. T.; Stack, T. D. P. *J. Am. Chem. Soc.* **2002**, *124*, 83−96.

(31) (a) Evans, D. F. *J. Chem. Soc.* **1959**, 2003−2005. (b) Löliger, J.; Scheffold, R. *J. Chem. Educ.* **1972**, *49*, 646−647. (c) Evans, D. F.; Jakubovic, D. A. *J. Chem. Soc., Dalton Trans.* **1988**, 2927−2933.

(32) Sheldick, G. M. *SHELXTL/PC for Windows XP*, version 6.12; Bruker AXS Inc.: Madison, WI, 2001.

(33) (a) Becke, A. D. *Phys. Rev. A* **1988**, *38*, 3098−3100. (b) Becke, A. D. *J. Chem. Phys.* **1993**, *98*, 1372−1377. (c) Becke, A. D. *J. Chem. Phys.* **1993**, *98*, 5648−5652. (d) Lee, C.; Yang, W.; Parr, R. G. *Phys. Rev. B* **1988**, *37*, 785−789.

(34) (a) Barone, V.; Cossi, M. *J. Phys. Chem. A* **1998**, *102*, 1995−2001. (b) Cossi, M.; Rega, N.; Scalmani, G.; Barone, V. *J. Comput. Chem.* **2003**, *24*, 669−681.

(35) Frisch, M. J. et al. *Gaussian 09*, revisions B.01 and D.01; Gaussian Inc.: Wallingford, CT, 2009.

(36) Ho, J.; Klamt, A.; Coote, M. L. *J. Phys. Chem. A* **2010**, *114*, 13442−13444.

(37) Yamaguchi, K.; Jensen, F.; Dorigo, A.; Houk, K. N. *Chem. Phys. Lett.* **1988**, *149*, 537−542.

(38) Wittbrodt, J. M.; Schlegel, H. B. *J. Chem. Phys.* **1996**, *105*, 6574−6577.

(39) Grimme, S. *J. Chem. Phys.* **2006**, *124*, 034108.

(40) Menon, A. S.; Radom, L. *J. Phys. Chem. A* **2008**, *112*, 13225−13230.